Title
Layilin Anchors Regulatory T Cells in Skin.

Journal
The Journal of Immunology, 207(7)

ISSN
0022-1767

Authors
Mehta, Pooja
Gouirand, Victoire
Boda, Devi P
et al.

Publication Date
2021-10-01

DOI
10.4049/jimmunol.2000970

Peer reviewed

HHS Public Access

Author manuscript

J Immunol. Author manuscript; available in PMC 2022 October 01.

Published in final edited form as:

J Immunol. 2021 October 01; 207(7): 1763–1775. doi:10.4049/jimmunol.2000970.

Layilin Anchors Regulatory T cells in Skin

Pooja Mehta[1,#], **Victoire Gouirand**[1,#], **Devi P. Boda**[1], **Jingxian Zhang**[1], **Sofia V. Gearty**[1], **Bahar Zirak**[1], **Margaret M. Lowe**[1], **Sean Clancy**[1], **Ian Boothby**[1], **Kelly M. Mahuron**[3], **Adam Fries**[2], **Matthew F. Krummel**[2], **Parminder Mankoo**[4], **Hsin-Wen Chang**[1], **Jared Liu**[1], **Joshua M. Moreau**[1], **Tiffany C. Scharschmidt**[1], **Adil Daud**[1], **Esther Kim**[3], **Isaac M. Neuhaus**[1], **Hobart W. Harris**[3], **Wilson Liao**[1], **Michael D. Rosenblum**[1,*]

[1]Department of Dermatology, University of California, San Francisco, 513 Parnassus Avenue, San Francisco, CA 94143, USA

[2]Department of Pathology, University of California, San Francisco, 513 Parnassus Avenue, San Francisco, CA 94143, USA

[3]Department of Surgery, University of California, San Francisco, 513 Parnassus Avenue, San Francisco, CA 94143, USA

[4]T-REX Bio. 863 Mitten Rd, Burlingame, CA 94010, USA

Abstract

Regulatory T cells (Tregs) reside in non-lymphoid tissues where they carry out unique functions. The molecular mechanisms responsible for Treg accumulation and maintenance in these tissues are relatively unknown. Using an unbiased discovery approach, we identified *LAYN* (layilin), a C-type lectin-like receptor, to be preferentially and highly expressed on a subset of activated Tregs in healthy and diseased human skin. Expression of layilin on Tregs was induced by TCR-mediated activation in the presence of IL-2 or TGFß. Mice with a conditional deletion of layilin in Tregs had reduced accumulation of these cells in tumors. However, these animals somewhat paradoxically had enhanced immune regulation in the tumor microenvironment, resulting in increased tumor growth. Mechanistically, layilin expression on Tregs had minimal effect on their activation and suppressive capacity *in vitro*. However, expression of this molecule resulted in a cumulative anchoring effect on Treg dynamic motility *in vivo*. Taken together, our results suggest a model whereby layilin facilitates Treg adhesion in skin, and in doing so, limits their suppressive capacity. These findings uncover a unique mechanism whereby reduced Treg motility acts to limit immune regulation in non-lymphoid organs and may help guide strategies to exploit this phenomenon for therapeutic benefit.

[*]**Address of Correspondence:** Michael D. Rosenblum M.D., Ph.D., Health Sciences West - 1201B, 513 Parnassus Avenue, San Francisco, CA 94132, Ph: 415-476-1685, Michael.Rosenblum@ucsf.edu.

Author Contributions

P.M. designed the studies, performed the experiments, and analyzed the data. P.M., V.G. and M.D.R. wrote the manuscript. V.G. performed and analyzed in vitro experiments with human Tregs. D.P.B, J.Z. and B.Z. assisted with experiments and data collection. S.G. and K.M.M. performed human skin flow cytometry studies. M.M.L. performed bulk RNA-seq data collection and analysis. A.F. and M.F.K. helped with 2-photon imaging, analysis and data interpretation. S.C. and M.M.L. performed Cytof studies. T.C.S. and S.G. helped in design and characterization of Layn$^{-/-}$ mouse. I.B. helped clone layilin overexpression vector. P. Mankoo, H.W.C., J.L. helped in RNAseq data analysis. J.M. provided critical feedback for in vitro experiments with human Tregs. E.K., I.M.N., A.D and H.W.H. provided human skin samples. W.L. provided critical feedback. M.D.R. oversaw all study design and data analysis. All authors discussed results and commented on the manuscript.

[#]Authors contribute equally

Keywords

Layilin; Regulatory T cells; Skin; Cellular Adhesion; Melanoma; Psoriasis

Introduction

Foxp3-expressing Regulatory T cells (Tregs) are a subset of $CD4^+$ T cells that play an essential role in establishing and maintaining immune homeostasis. Populations of these cells stably reside in both lymphoid organs and in specific peripheral (non-lymphoid) tissues. It is becoming increasingly appreciated that Tregs that reside outside of the lymphoid compartment have distinct functions that are largely dependent on their tissue microenvironment (1). Tregs resident in visceral adipose tissue play a role in metabolism (2), Tregs in lungs and skeletal muscle prevent injury and facilitate tissue repair (3–5) and Tregs in skin promote epithelial barrier regeneration, facilitate hair follicle cycling and limit fibrosis (6–8). Because Tregs are thought to mediate many of their functions in the tissues in which they reside, and optimal therapeutic approaches directed at either augmenting or inhibiting these cells will most likely require strategies that target specific subsets, it is of fundamental importance to further define the molecular pathways utilized by these cells in tissues.

Lymphocytes that stably reside in non-lymphoid organs express specific adhesion molecules that enable their steady-state maintenance and facilitate motility within the tissue during normal organ function. In skin, a large subset of Tregs preferentially localize to hair follicles (9–11) and the abundance of these cells fluctuates with the hair follicle cycle (6). In addition to adhesion molecules, the majority of tissue resident Tregs express relatively high levels of Treg ‘effector’ molecules known to play important roles in immune regulation, including Foxp3, CTLA-4, CD25 and ICOS (6, 11–13). Interestingly, cellular adhesion and activation are intricately linked. Molecular pathways that primarily mediate adhesion can promote lymphocyte activation, with the best example being integrin-mediated augmentation of T cell receptor signaling during antigen engagement in the immunological synapse (14). Alternatively, signaling through adhesion receptors can initiate and/or augment negative feedback loops that attenuate cell activation (15). For example, specific integrins inhibit myeloid cell and platelet activation during TLR stimulation (16–19) , while at the same time promoting cellular adhesion. In addition, members of the C-type lectin family of cell surface receptors inhibit immune cell activation in specific physiologic settings (20). Currently, very little is known about how adhesion molecules influence Treg activation and suppressive capacity in peripheral tissues and skin.

In an attempt to define adhesion molecules preferentially utilized by Tregs in skin, we compared the transcriptome of these cells to other tissue-resident immune and non-immune cell subsets. We discovered that *LAYN*, the gene encoding for layilin, is selectively expressed in subsets of highly activated Tregs resident in this tissue. Layilin is a C-type lectin-like surface receptor that interacts with the actin cytoskeleton and mediates cellular adhesion (21–23). Recently, we discovered that layilin facilitates $CD8^+$ T cell adhesion

through modulation of talin-binding integrins, including LFA-1 (24). In the current study, we sought to determine the potential role of this pathway in influencing skin-Treg biology.

Materials and Methods

Experimental Animals

C57BL/6J wild-type (WT), Foxp3^{DTR} mice, Foxp3^{GFP}, CD45.1;Foxp3$^{ERT2\text{-}GFPCre}$ and Rag2$^{-/-}$ mice were purchased from The Jackson Laboratory (Bar Harbor, ME) and were bred and maintained in the University of California San Francisco (UCSF) specific pathogen-free facility. Mice with a germ-line deletion of layilin (Layn$^{-/-}$) were created using a CRISPR-Cas9 approach (25). Guide RNAs were designed to target exons 1 and 4 and delivered with Cas9 into C57BL/6 embryos (Supplementary Figure S2A). Three founder lines were generated: 2 with deletions from exon 1 to 4 and one with a SNP in exon 4, resulting in a premature stop codon. Founder pups generated were back-crossed to wildtype C57BL/6 mice (over 2 generations) to establish layilin-deficient (Layn$^{-/-}$) mouse lines. Layn$^{fl/fl}$ mice were created by inserting LoxP sites flanking exon 4 of layilin gene using CRISPR-Cas9. Layilin was deleted specifically on Tregs by crossing Layn$^{fl/fl}$ mice to Foxp3$^{ERT2\text{-}GFPCre}$ mice, upon treatment with tamoxifen. All mouse experiments were performed on 7–12 week old animals. All mice were housed under a 12-hour light/dark cycle. All animal experiments were performed in accordance with guidelines established by Laboratory Animal Resource Center at UCSF and all experimental plans and protocols were approved by IACUC beforehand.

Human specimens

Normal healthy human skin was obtained from patients at UCSF undergoing elective surgery, specimens received were deidentified and certified as Not Human Subjects Research. Blood samples were obtained from healthy adult volunteers (study number 12–09489). Biopsies of accessible melanoma tumors were obtained with a 16- or 18-gauge needle, or a 4-mm punch biopsy tool (study number 138510). Biopsies of psoriasis were obtained with a 6-mm punch biopsy tool (study number 10–02830). For all fresh human tissue samples, active/flaring disease was confirmed both clinically and histologically. Studies using human samples were approved by the UCSF Committee on Human Research and by the IRB of UCSF. Informed written consent was obtained from all patients.

Human Skin Digestion

Skin samples were stored in a sterile container on gauze and PBS at 4°C until the time of digestion. Skin was processed and digested as previously described (11). Briefly, hair and subcutaneous fat were removed, and skin was cut into small pieces and mixed with digestion buffer containing 0.8 mg/ml Collagenase Type 4 (4188; Worthington), 0.02 mg/ml DNAse (DN25–1G; Sigma-Aldrich), 10% FBS, 1% HEPES, and 1% penicillin/streptavidin in RPMI medium and digested overnight in an incubator. They were then washed (2% FBS, 1% penicillin/ streptavidin in RPMI medium), double filtered through a 100-μm filter, and cells were pelleted and counted. Human PBMCs were prepared by Ficoll-Paque gradient centrifugation. Single cell suspensions were then stained with antibodies for flow cytometric analysis or FACS sorting.

RNA-Sequencing Analysis of Tregs and Teff cells

Treg cells were isolated by gating on live $CD45^+CD3^+CD4^+CD8^-CD25^{hi}CD27^{hi}$ cells, which contained greater than 90% Foxp3-expressing Tregs. Teff cells were isolated by gating on live $CD45^+CD3^+CD4^+CD8^-CD25^{low}CD27^{low}$ cells, which contained less than 1% Foxp3-expressing Tregs. Sort-purified cell populations were flash frozen in liquid nitrogen and were shipped overnight on dry ice to Expression Analysis, Quintiles (Morrisville, NC). RNA samples were converted into cDNA libraries using the Illumina TruSeq Stranded mRNA sample preparation kit. (Illumina). RNA was isolated using Qiagen RNeasy Spin Column and was quantified via Nanodrop ND-8000 spectrophotometer. The quality of RNA was checked using Agilent Bioanalyzer Pico Chip. 220 pg of input RNA was used to create cDNA using the SMARTer Ultra Low input kit. Samples were sequenced using Illumina RNA-Seq to a 25M read depth. Reads were aligned to Ensembl hg19 GRCh37.75 reference genome using TopHat software (v. 2.0.12) (26) and SAM files were generated using SAMtools (27). Read counts were obtained with htseq-count (0.6.1p1) with the union option (Anders et al., 2015). The R/Bioconducter package DESeq2 was used to determine differential expression (28).

RNA-Sequencing Analysis of Tregs, Teff cells, $CD8^+$ T cells, dendritic cells and keratinocytes from healthy human skin

Cells were sorted and analyzed as described previously (29). Tregs and Teffs were sorted as described above. Expression of layilin was analyzed by ANOVA.

Treg activation assay and induction of layilin expression on Tregs derived from human peripheral blood

Tregs were sort purified (as described above) from peripheral blood of healthy volunteers. Purified Tregs were *ex vivo* expanded as previously described (30). Briefly, cells were cultured for 14 days in complete X-Vivo media (Lonza) with 500U/ml IL-2 (2000U/ml, Tonbo Biosciences) and stimulated with anti-CD3/CD28 beads at cells:beads ratio of 1:1 (Gibco). On day 14, cultures were rested overnight in X-Vivo media only and 10,000 cells were washed and stained for baseline. 200,000 cells were plated in in a 96 well U-bottom plate and re-stimulated with anti-CD3/CD28 beads. Layilin antibody or cytokines were added at the same time using the following concentrations: 25ug/ml LAYN (1mg/ml, Sinobiological) 10ng/ml IL-15 (50ug/ml, R&D systems), 5ng/ml TGF-β (10ug/ml, Peprotech), and/or 500U/ml IL-2. After 3 days of incubation, cells were washed, stained and analyzed using flow cytometry. Expression of activation markers and layilin was quantified based on isotype control antibody or secondary control and analyzed by one-way ANOVA and corrected with a Bonferroni test.

Mass Cytometry

Single cell suspensions were obtained from 4 mm punch biopsies of psoriatic lesions. Cells were first washed with 5 mM EDTA-PBS and centrifuged at 600 g for 5 minutes at 4 °C. Cells were then resuspended with equal volumes of 5 mM EDTA-PBS and 50 uM cisplatin (Sigma, P4394) for 1 minute at room temperature (RT) before quenching with 5 mM EDTA-PBS with 0.5% BSA. After centrifugation, cells were fixed with 1.6%

PFA in PBS with 0.5% BSA and 5 mM EDTA for 10 minutes at RT and then washed twice with PBS. Cells were then resuspended in PBS with 0.5% BSA and 10% DMSO and stored at −80 °C. Prior to staining, cells were left to thaw at RT and washed in Cell Staining Media (CSM, PBS with 0.5% BSA and 0.02% NaN3) and then vortexed with FC Receptor Blocking Solution (BioLegend, 422302). LAYN (Sino Biological, 10208-MM02), PD-1 (BioLegend, EH12.2H7), and CD8a (BioLegend, RPA-T8) antibodies were metal-conjugated at the UCSF Parnassus Flow Cytometry Core using Maxpar Antibody Labeling Kits (Fluidigm). All other metal conjugated antibodies were obtained from Fluidigm. Cells were stained as previously described (31). Briefly, cells were stained in an extracellular antibody cocktail for 30 minutes at RT on a shaker and then washed with CSM. Cells were then permeabilized with the Foxp3/Transcription Factor Staining Buffer Set (eBioscience, 00-5523-00) for 30 minutes at RT on a shaker and then washed twice with Permeabilization Buffer (eBioscience, 00-8333-56) before staining in an intracellular antibody cocktail for 1 hour at RT on a shaker. Following intracellular staining, cells were washed once with Permeabilization Buffer and once with CSM, and then resuspended in PBS with 1.6% PFA and 100 nM Cell-ID Intercalator-Ir (Fluidigm, 201192B) and kept at 4 °C. Before data acquisition, cells were washed sequentially in CSM, PBS, and MilliQ H_2O. Cells were then resuspended in MilliQ H_2O containing EQ Four Elements Calibration Beads (Fludigm, 201078) and analyzed with a CyTOF2 Mass Cytometer (Fluidigm). Mass cytometry files were normalized to the bead standards (32) in R (3.6.1) using the premessa package (0.2.4, github.com/ParkerICI/premesa). Analysis was performed on viable singlets as determined by the iridium, event length, and cisplatin channels. UMAP visualizations were generated with the CATALYST package (33) (1.10.1) using CD4+ cells (CD45+CD3+CD4+CD8-) exported manually from biaxial plots in FlowJo (10.6.1) and clusters were based on expression of CD25, FOXP3, CTLA4, CD27, and CD127.

Tumor Growth Experiments

MC38 colon adenocarcinoma model was performed as previously described (34). Briefly, 5×10^5 MC38 tumor cells (Kerafast) resuspended in 200ul of PBS were injected subcutaneously into the right flank of mice. Tumor diameters were measured every 2–3 days using electronic calipers and the tumor volume was calculated using the formula $V = (L*W^2)/2$ (35). Tumor Infiltrating Lymphocytes (TILs) were isolated by harvesting tumors after 2–4 weeks, and mincing and digesting them similar to the skin.

Mouse Tissue Processing

Isolation of cells from axillary, brachial and inguinal lymph nodes (referred to as skin draining lymph nodes, sdLNs) and spleen for flow cytometry was performed by mashing tissue over sterile wire mesh. Mouse skin was digested and single cells suspensions prepared as previously described (36). Briefly, skin was minced and digested in buffer containing collagenase XI, DNase and hyaluronidase in complete RPMI in an incubator shaker at 225 rpm for 45 minutes at 37°C. An automated cell counter (NucleoCounter NC-200, Chemometec) was used to count cell numbers. $2–4 \times 10^6$ cells were stained and flow cytometric analysis performed.

Flow Cytometry

Single-cell suspensions were counted, pelleted and incubated with anti-CD16/anti-CD32 Fc block (BD Biosciences; 2.4G2). Cells were washed and stained with Ghost Viability dye (Tonbo Biosciences) and antibodies against surface markers in PBS. For intracellular staining, cells were fixed and permeabilized using a FoxP3 staining kit (eBioscences) and then stained with antibodies against intracellular markers. Fluorophore-conjugated antibodies specific for human or mouse surface and intracellular antigens were purchased from BD Biosciences, eBiosciences or Biolegend. The following anti-mouse antibodies and clones were used: CD3 (145–2C11), CD4 (RM4–5), CD8 (53–6.7), CD45 (30-F11), FoxP3 (FJK-16s), TCRb (H57–597), CD25 (PC61.5), CD45.1 (A20), CD45.2 (104), CTLA4 (UC10–4B9), ICOS (C398.4A), Ki67 (B56), LAG3 (C9B7W), 41BB (17B5), PD1 (10F.9G2), IFNγ (XMG1.2), TNFα (MP6-XT22), Ly6G (1A8), F4/80 (BM8), CD11b (M1/70), MHC class II (M5/114.15.2), Ly6C (HK1.4), CD206 (C068C2), CD11c (N418). The following anti-human antibodies and clones were used: layilin (LS Bio 4C11), PE-Streptavidin, CD3 (UCHT1), CD4 (SK3), CD8 (SK1), CD45 (HI30), FoxP3 (PCH101), CD25 (M-A251), CTLA4 (14D3), ICOS (ISA-3), CD27 (LG.7F9), CD11c (3.9), HLA-DR (L243), 41BB (4B4–1), PD1 (EH12.2H7), Ki67 (EH12.2H7), LAG3 (11C3C65). Layilin Ab was biotin-tagged using Miltenyi's One-Step Antibody Biotinylation kit (130-093-385). Samples were run on a Fortessa analyzer (BD Biosciences) in the UCSF Flow Cytometry Core and data was collected using FACS Diva software (BD Biosciences). Data were analyzed using FlowJo software (FlowJo, LLC). Dead cells and doublet cell populations were excluded, followed by pre-gating on $CD45^+$ populations for immune cell analysis. Lymphoid cells were gated as $TCR\alpha\beta^+CD3^+$ αβ T cells, $CD3^+CD8^+$ T cells (CD8), $CD3^+CD4^+CD25^-Foxp3^-$ T effector cells (Teff), and $CD3^+CD4^+CD25^+Foxp3^+$ regulatory T cells (Treg).

Ex Vivo Expansion and Retroviral Transduction of Mouse Tregs

Spleens and sdLN were harvested and lymphocytes isolated from congenically-marked CD45.1 C57BL/6 mice. Total $CD4^+$ T cells were isolated using EasySep magnetic bead enrichment kit (StemCell Technologies). Tregs were sort-purified by gating on $CD4^+CD25^{hi}$ cells, which were >95% $Foxp3^+$, using Aria (BD Biosciences). In all experiments, purity of Tregs was >95%. Sorted Tregs were *ex vivo* expanded by methods previously described (30). Briefly, Tregs were cultured in complete DMEM with IL-2 (2000U/ml, Tonbo Biosciences) and stimulated with mouse anti-CD3/CD28 beads at cells:beads ratio of 1:3 (Dynabeads, Thermo Fisher). On day 2, cells were retrovirally transduced with either control empty-eGFP-pMIG vector or Layilin-eGFP-pMIG vector at multiplicity of infection of 1 by spinoculation at 6000g for 90 minutes at 25°C. Cells were then cultured and collected on day 5. On the day of collection, transduction efficiency (as measured by % of GFP^+ cells) was checked by flow cytometry. Transduction efficiencies were routinely between 70% and 90% and were similar for empty vector and vector encoding Layilin and used to normalized experiment readout. Also, an aliquot of cells were pelleted and frozen for later Layn mRNA analysis by qPCR.

In vitro mouse Treg assays

To setup *in vitro* Treg suppression assay, sorted mouse Tregs, overexpressing either empty vector or Layilin-eGFP-pMIG vector, were cocultured with CellTrace Violet-labeled Teffs at varying proportions, along with mitomycin C-treated TCRb-depleted splenocytes (Antigen Presenting Cells) and soluble α-CD3ε (0.5ug/ml) for 72 hours at 37°C as previously described (37). These experiments were carried out in triplicates/condition in a 96 well U-bottom plate precoated with mouse skin fibroblasts, as a potential source of ligand for layilin. Mouse skin fibroblasts were obtained by digesting the whole skin in presence of collagenase + DNase and culturing the cells in fibroblast growth medium (Promocell) for 5–7 days to enrich for fibroblasts. Teffs were analyzed for CTV dilution by flow cytometry.

Skin-wounding assays and analysis

Four full-thickness excisional wounds were generated with a 4-mm sterile punch (Stiefel Laboratories, Research Triangle Park, NC) after depilation. Wounds were photographed and wound area was measured with image analysis software (ImageJ 1.64v). The surface area of wound defects was expressed as a percentage of closure, relative to the initial surface of each wound.

Adoptive Transfer of Layilin-overexpressing Tregs into Foxp3^{DTR} mice

D9 Treg cells, retrovirally transduced to overexpress layilin. 2.5 – 3.5 × 10^5 cells re-suspended in PBS, were adoptively transferred into Foxp3^{DTR} mice via retro-orbital injection. One control group (no Treg) was not injected with Treg cells to validate full Tregs CD45.2 depletion after Diphtheria toxin (DT) injection. 3 days after adoptive transfer of cells, first DT injection was given and then DT was injected every other day for a total of 5 doses. The optimal dose for each DT lot (Sigma-Aldrich) was previously determined by measuring the efficiency of skin Treg depletion by flow cytometry. Accordingly, Foxp3^{DTR} mice were injected with DT intraperitoneally at 30ng/g body weight. Mice were sacrificed and skin and sdLN were harvested 13–14 days post-transfer. All flow cytometry data have been normalized to transfection efficacy measured at D5.

Intravital Two-Photon Microscopy and Image Analysis

Instrumentation for two-photon imaging has been previously described (38). Dorsal skin imaging using two-photon microscopy was done as previously described (6). Briefly, albino mice were anesthetized using isoflurane, hair on dorsal skin was shaved and depilated, and mice were then placed on a custom heated microscope stage. The depilated skin was gently immobilized using a custom suction window and an embedded 12mm coverslip (39). The microscope stage was then lifted to be right above a water-immersion objective lens (Olympus 25x, 1.05 numerical aperture). Fluorescence excitation was achieved by a Spectra-Physics MaiTai Ti-Saphire Laser tuned to 890 nm for excitation of GFP. Collagen was visualized using second harmonic signals. Z-stack images were acquired with a vertical resolution of 2μm for a total of 80–100μm depth. For collecting a time-series of images, three-dimensional stacks were acquired every 5 minutes using Micro-Magellan (40). Raw imaging data were processed using ImageJ Software. Images were analyzed, corrected for motion, and cells were tracked by rendering 3D surfaces and spots over the cells using

Imaris Software (Bitplane). To determine *in vivo* changes in Treg cell shape, the sphericity of individual Tregs was calculated over the time-lapse period, as previously described (39).

Quantitative PCR

For assessment of Layilin gene expression, Tregs and Teffs were sort-purified from skin and sdLNs of WT mice and RNA isolated using a column-based kit (PureLink RNA Mini Kit, Thermo Fisher). RNA was then transcribed (iScript cDNA synthesis Kit, Bio-Rad) and pre-amplified (SSo Advanced PreAmp Supermix, Bio-Rad). Expression of Layilin was determined using a SYBR Green assay (SSo Advanced Universal SYBR Green kit; Biorad). Cycle number of duplicate or triplicate samples were normalized to the expression of the endogenous control β2m. Primer sequences or assay ids used are as follows: β2m (For: 5' – TTCTGGTGCTTGTCTCACTGA – 3'; Rev 5' – CAGTATGTTCGGCTTCCCATTC - 3'), mouse Layilin (qMmuCID0022543, Biorad). Data are presented as negative fold change of Delta-Delta CT or as standardized arbitrary units (AU).

Statistical Analyses

Statistical analyses were performed with Prism software package version 6.0 (GraphPad). P values were calculated using two-tailed unpaired or paired Student's *t*-test, unless specified otherwise. Pilot experiments were used to determine sample size for animal experiments. No animals were excluded from analysis, unless due to technical errors. Mice were age- and gender-matched and randomly assigned into experimental groups. Appropriate statistical analyses were applied, assuming a normal sample distribution. All *in vivo* mouse experiments were conducted with at least 2–3 independent animal cohorts. RNA-Seq experiments were conducted using 4–5 biological samples (as indicated in figure legends). Data are mean ± S.E.M. P values correlate with symbols as follows: ns = not significant, $p>0.05$, *$p<0.05$, **$p<0.01$, ***$p<0.001$, ****$p<0.0001$.

Results

A subset of highly activated Tregs express layilin in healthy and diseased human skin

To elucidate molecular pathways that are unique to Tregs in human skin, we performed whole transcriptome RNA sequencing (RNAseq) on Tregs and $CD4^+$ effector T (Teff) cells sort-purified from normal human skin (Figure 1A). Using this unbiased discovery approach, we identified *LAYN* to be preferentially expressed by Tregs as compared to Teff cells in skin (Figure 1A–C). The fold change in gene expression was comparable to that of Foxp3, the master regulator of Treg development and function (41). To ensure we had effectively purified Tregs, we confirmed differential expression of the 'core Treg signature' (42) between the two cell subsets, including CD25, CTLA-4 and CD27 (Figure 1B and data not shown). To determine if layilin expression was unique to Tregs in human skin, we sort-purified Tregs, $CD4^+$ Teff cells, $CD8^+$ T cells, dendritic cells and keratinocytes from skin of a separate cohort of normal healthy donors and performed whole transcriptome RNAseq analysis. We found that Tregs preferentially express high levels of layilin when compared to all other cell populations evaluated (Figure 1D). To validate our RNAseq findings, we measured expression of layilin protein by flow cytometry on $CD4^+$ T cells in skin of normal healthy individuals and compared expression to these cells in peripheral

blood (Figure 1E). Consistent with our RNAseq results, layilin was highly expressed on skin Tregs compared to skin Teff cells. Although a small fraction of Tregs in peripheral blood expressed layilin (~1–3%), approximately 40% of Tregs in skin expressed high levels of this protein (Figure 1E). Interestingly, not all Tregs in skin expressed layilin at the protein level. This was not a result of enzymatic digestion of the epitope during skin cell preparation (data not shown), confirming that only a subset of skin Tregs express layilin in normal human skin in the steady-state. To better define the layilin-expressing Treg subset, we quantified the expression of Treg activation/functional markers such FOXP3, CD25, CTLA4, ICOS and CD27 on layilin^{+} and layilin^{-} Tregs in healthy human skin. Layilin^{+} Tregs expressed significantly higher levels of all these Treg 'effector' molecules (Figure 1F).

To determine if layilin expression was maintained on Tregs in diseased human skin we analyzed tumors from patients with metastatic melanoma and skin of patients with psoriasis. Whole transcriptome RNAseq was performed on sort-purified Tregs and Teff cells in a similar fashion to that described for normal skin. We found that Tregs infiltrating metastatic melanoma tumors and psoriasis skin express significantly higher levels of layilin as compared to CD4^{+} Teff cells (Figure 1G–L). Mass cytometric (CyTOF) analysis of immune cell infiltrates in psoriatic skin revealed that layilin expression correlated with the most 'activated' Tregs (Figure 1M). Similar findings were observed on Tregs infiltrating human melanoma, as quantified by standard flow cytometry (Supplementary Figure S1A). Taken together, these results suggest that layilin is preferentially expressed on a subset of highly activated Tregs in healthy and diseased human skin, with minimal expression on Tregs in peripheral blood and other immune and non-immune cell types.

Layilin was highly expressed on a subset of Tregs in healthy human skin and minimally expressed on Tregs in peripheral blood (Figure 1A–D). In addition, the overwhelming majority of Tregs in both murine and human skin have a tissue-resident memory (Trm) phenotype (6, 8, 11). We hypothesized that cytokines that establish and/or maintain Trm cells may induce layilin expression. Both TGF-ß and IL-15 play dominant roles in controlling Trm homeostasis in tissues, especially in skin (43–45). Thus, we tested the potential of both of these cytokines to induce layilin expression on Tregs. CD25^{hi}CD127^{lo} CD4^{+} T cells (>90% Foxp3^{+}) were sort purified from peripheral blood of 3 healthy donors and expanded *ex vivo* for 14 days with anti-CD3/anti-CD28 coated beads and high dose IL-2 per standard protocol (30). Cells were then rested in media and re-stimulated for 3 more days in the presence of optimal concentrations of IL-2, IL-15 or TGF-ß, and layilin expression quantified by flow cytometry. Because *ex vivo* expanded Tregs are dependent on IL-2, both IL-15 and TGF-ß were added with or without IL-2. Initial Treg activation and expansion *via* TCR stimulation, CD28-mediated co-stimulation and IL-2 induced layilin expression, with approximately 35–60% of Tregs expressing layilin after 14 days of culture ('baseline'; Supplementary Figure S1B–C & data not shown). As expected, Treg re-stimulation with high dose IL-2 significantly enhanced layilin expression over this baseline (Supplementary Figure S1B–C). However, this was not observed with IL-15, and the addition of IL-2 with IL-15 did not rescue layilin induction. In contrast, the addition of TGF-ß resulted in a significant induction of layilin expression, comparable to that of high dose IL-2, and the combination of IL-2 with TGF-ß did not enhance layilin expression over TGF-ß alone (Supplementary Figure S1B–C). Taken together, these results suggest that

Treg activation/expansion in the presence of IL-2 is sufficient to induce layilin on peripheral blood derived Tregs, and that TGF-ß and not IL-15 enhances layilin expression on these cells.

Layilin attenuates Treg suppressive capacity in vivo

To determine if layilin influences Treg suppressive capacity, we first confirmed that expression in mice mirrored that of humans. Using a qRT-PCR approach (anti-layilin antibodies are currently not available in mice) we confirmed layilin expression in skin Tregs with minimal expression on Tregs in secondary lymphoid organs and skin-resident Teff cells (Supplementary Figure S2A). Next, we generated a mouse strain in which *Layn* could be conditionally deleted in specific cell types (*i.e., Layn*$^{flox/flow}$ mice). We recently reported the first studies using this mouse strain in CD8^{+} T cells (24). Briefly, flox sequences were inserted to flank exon 4 of the layilin gene using CRISPR/Cas9 technology (46). This results in complete deletion of exon 4, corresponding to the C-type lectin domain of *LAYN,* when crossed to mice expressing Cre-recombinase in specific cell lineages (47) (Supplementary Figure S2B). To elucidate the function of layilin on Tregs, we crossed *Layn*$^{flox/flox}$ mice to Foxp3$^{ERT2\text{-}GFP\text{-}Cre}$ mice (49) (Foxp3^{Cre}Layn$^{fl/fl}$) in which layilin can be induced to be deleted in adult animals in Tregs (upon treatment with tamoxifen), respectively (Supplementary Figure S2B–C). Both Foxp3^{Cre}Layn$^{fl/fl}$ mice developed normally and did not have any gross defects in total leukocyte numbers in skin and skin-draining lymph nodes (sdLN) (Supplementary Figure S2D). Treg numbers and phenotype in skin in Foxp3$^{ERT2\text{-}Cre}$Layn$^{fl/fl}$ mice after treatment with tamoxifen were normal when compared to untreated gender- and age-matched control mice, suggesting that layilin is not required for accumulation and/or maintenance in murine skin in the steady state (Supplementary Figure S2E–F).

Because layilin is expressed on Tregs infiltrating human tumors (Figure 1G–I and (50–52)) and these cells have been shown to influence tumor growth and metastasis (53, 54), we set out to determine if Treg expression of layilin influences tumor growth in the MC38 colon adenocarcinoma model. This model was chosen because it is relatively immunoresponsive where Tregs play a significant role (53, 54). At early time point of the tumor progression where no difference between the two groups are observed (D13), layilin on Treg do not appear as required for the establishment of the tumor (Supplementary Figure 2G–L). However, once tumor is well established, when compared to Foxp3^{Cre} control mice treated with tamoxifen, Foxp3^{Cre}Layn$^{fl/fl}$ mice upon treatment with tamoxifen had significantly increased tumor volumes and growth kinetics (Figure 2A). Quantification of tumor immune cell infiltrates revealed a significant reduction in IFNγ-producing CD8^{+} T cells and reduced proliferative (Ki67^{+}) CD8^{+} T cells in Foxp3^{Cre}Layn$^{fl/fl}$ mice compared to controls (Figure 2B). Similar results were observed in the CD4^{+} Teff compartment (Figure 2C). In addition, Ly6C^{high} pro-inflammatory tumor-infiltrating macrophages were significantly reduced in Foxp3^{Cre}Layn$^{fl/fl}$ mice with a concomitant increase in CD206^{high} anti-inflammatory macrophages (Figure 2D).

Given that layilin plays a role in mediating cellular adhesion to the ECM (23, 24, 47), we set out to determine whether this pathway influenced Treg accumulation in tumors.

Layilin-deficient Tregs (in $Foxp3^{Cre}Layn^{fl/fl}$ mice) were reduced in percentage and absolute numbers in tumors when compared to control mice (Figure 2E). This was primarily observed in tumors, as there were no differences in absolute numbers of Tregs in tumor draining lymph nodes (DLNs) and adjacent uninvolved skin between $Foxp3^{Cre}Layn^{fl/fl}$ mice and $Foxp3^{Cre}$ controls (Figure 2E). There was a slight decrease in the percentage of Tregs in tumor DLNs in $Foxp3^{Cre}Layn^{fl/fl}$ mice. Taken together, these results suggest that layilin expression on Tregs facilitates their accumulation in tumors. However, somewhat paradoxically, this culminates in a less suppressive tumor microenvironment.

Layilin plays a minor role in Treg-mediated suppression in vitro

We next set out to determine the mechanisms by which layilin influences Treg function. It is possible that layilin binding to the ECM mediates an inhibitory signal, resulting in enhanced accumulation of less suppressive Tregs. Alternatively, layilin binding to the ECM may primarily act to limit Treg motility, resulting in diminished suppressive capacity secondary to reduced ability to interact with (and thus regulate) other immune cells in the tissue microenvironment. To determine if layilin attenuates Treg suppressive capacity in a cell-intrinsic manner, we over-expressed this protein on murine Tregs. Consistent with our finding that layilin is minimally expressed on Tregs in human peripheral blood (Figure 1E), we found that Tregs isolated and expanded from murine secondary lymphoid organs (*i.e.,* spleen and lymph nodes) express minimal amounts of layilin (Supplementary Figure S2A and S1C), thus providing an ideal cell source to determine how layilin expression influences Treg function. We employed a retroviral transduction approach to express mouse layilin on Tregs (mLayn-Tregs) isolated from sdLN and spleen. Control Tregs were transduced with empty vector-eGFP (EV-Tregs). The efficiency of transduction was routinely ~70–90%, as measured by GFP expression and GFP^+ cells were highly pure Tregs (Supplementary Figure S3A–B). Without affecting FOXP3 MFI, mLayn-transduced cells expressed significantly higher levels of layilin mRNA when compared to untransduced Tregs even after TCR stimulation using anti-CD3/CD28 beads (Supplementary Figure S3C–D). Congenically disparate CellTrace Violet (CTV)-labeled CD4+ Teffs were stimulated with α-CD3 and irradiated APCs in the presence of mLayn-Tregs or control EV-Tregs. These assays were performed on plates pre-coated with syngeneic dermal fibroblasts, to provide extracellular matrix as a physiologic ligand for layilin (55) (Figure 3A). In these experiments, Tregs over-expressing layilin had slightly reduced suppressive capacity, only observed at higher Treg to Teff ratios (Figure 3B). Proliferation of Teffs, as measured by Ki67 staining and CTV-based division index, was found to be marginally higher in Teffs cocultured with mLayn-Tregs (Figure 3B and Supplementary Figure S3E). Layilin overexpression did not affect Treg activation markers such as Foxp3, CD25, 4–1BB and LAG3 in these assays (Figure 3C). Taken together, these results suggest that layilin minimally attenuates Treg suppressive capacity *in vitro*.

Crosslinking layilin on human Tregs does not impact Treg activation

In the experiments described above, layilin was exogenously expressed on murine Tregs isolated from secondary lymphoid organs. In this system, layilin is most likely expressed at supraphysiologic levels on cells that do not normally express this protein. In addition, it is difficult to quantify whether productive interactions occur between layilin and the ECM in

these experiments. To circumvent these potential caveats, we established a system whereby human Treg activation could be quantified after crosslinking layilin on cells that naturally express this receptor (Figure 4A). Tregs sort purified from peripheral blood and expanded *ex vivo* with α-CD3/CD28 coated beads and high dose IL-2 begin to express layilin at appreciable levels after 5 days in culture and express maximal levels on days 5 and 12 (Figure 4B). To determine if signaling through layilin influences Treg activation, we used an anti-human layilin antibody that we have previously shown to engage and cross-link this receptor (24). Tregs were expanded from several donors for 9 or 14 days, and then re-stimulated at day 9 or day 14 with or without α-CD3/CD28 beads and a saturating dose of anti-layilin antibody. Three days later, Treg activation markers were quantified by flow cytometry. In these experiments, crosslinking layilin on Tregs had no effect on Treg activation, as measured by mean fluorescence intensity and percentage of cells expressing Foxp3, CD25, ICOS, 4–1BB, LAG3 and Ki67 (Figure 4C and data not shown). Taken together, these results are consistent with data obtained in our murine suppression assays and suggest that engaging layilin on Tregs has minimal direct effect on the activation and thus suppressive capacity of these cells *in vitro*.

Layilin expression on Tregs enhances their accumulation in inflamed skin

The results described above suggest that the primary function of layilin is most likely not to provide a direct signal to Tregs to attenuate their activity. Instead, it is possible that layilin mediated adhesion to the ECM *in vivo* acts to anchor these cells, and in doing so, limits their ability to interact with and regulate other immune cells in tissues. To begin to test this hypothesis, we first set out to determine if layilin facilitates Treg adhesion in skin as it does in tumors. To this end, we utilized a skin-wound healing assay we have previously shown that Tregs facilitate full thickness skin wound healing by suppressing inflammation early after wounding (56). To determine whether layilin expression on Tregs plays a role in skin-specific inflammation, we induced full thickness skin wounds of $Foxp3^{Cre}$ or $Foxp3^{Cre}Layn^{fl/fl}$ mice with layilin deleted in Tregs and measured wound closure. In these experiments, we observed a significant attenuation in wound healing in these mice compared to controls (Supplementary Figure S3F). This result showing the importance of layilin in a skin-inflammation context, we pursued with a well-established systemic model of inflammation of Treg adoptive transfer model into Foxp3-DTR hosts (57–59). In this system, endogenous Tregs are depleted through administration of diphtheria toxin and syngeneic Tregs adoptively transferred to replenish the Treg compartment. We adoptively transferred mLayn- or EV-transduced Tregs (isolated and expanded from secondary lymphoid organs as described above) into $Foxp3^{DTR}$ mice (60) and Tregs were depleted for 10 days. Skin was then harvested for flow cytometric quantification of relative Treg abundance (Figure 5A). Metrics of Treg proliferation and survival were also quantified. In these experiments, we observed a pronounced and significant increase in the accumulation of mLayn-Tregs in skin compared to control EV-Tregs (Figure 5B). There was a preferential accumulation of transduced (*i.e.*, GFP^+) cells in the total $CD45.1^+$ transferred population in the mLayn-transduced group compared to the EV-transduced control group (Figure 5C), suggesting that layilin expression (and not the transduction process itself) correlates with increased tissue Treg accumulation. Interestingly, we did not observe any differences in the proliferative index (as measured by percentage of Tregs expressing Ki67)

between mLayn- and EV-transduced Tregs either early or late post-transfer (Figure 5D and data not shown). In addition, the percentage of dead cells within the CD45.1^{+} gate was equal between the two groups both early and late post-adoptive transfer (data not shown). These results suggest that migration to and/or retention in skin is the primary mechanism by which layilin-expressing Tregs preferentially accumulate.

Enhanced Treg accumulation in the experiments described above could be secondary to a more inflammatory environment created by layilin-expressing cells. To test whether layilin-mediated Treg accumulation was cell-intrinsic or dependent on the tissue microenvironment, we performed competitive adoptive transfer experiments. Congenically labeled mLayn- and EV-transduced Tregs were mixed in a 1:1 ratio and co-adoptively transferred into the same Foxp3^{DTR} host mice depleted of endogenous Tregs (Supplementary Figure S3G). After 10 days of Treg depletion, skin was harvested and Treg accumulation quantified by flow cytometry. Consistent with experiments where Tregs were transferred into separate hosts, we observed significantly enhanced accumulation of layilin-expressing Tregs relative to EV controls in skin of co-adoptively transferred animals (Supplementary Figure S3H). Additionally, there was no significant difference in Ki67 expression between mLayn- and EV-transduced Tregs either early or late after adoptive transfer (Supplementary Figure S3I and data not shown). There was also no significant difference in the percentage of dead Tregs between the 2 cell populations (Supplementary Figure S3J). Taken together, these results suggest that layilin promotes the *in vivo* accumulation of Tregs in skin in a cell-intrinsic fashion, and that this is most likely not secondary to enhanced proliferation or survival.

Layilin Functions to ‘Anchor’ Tregs in skin

To further discern the mechanism by which layilin influences Treg accumulation in skin, we performed intravital tissue imaging of these cells. Because the YFP and GFP intensities in Foxp3^{Cre} and Foxp3$^{ERT2\text{-}Cre}$ mice are too weak to be reliably detected by 2-photon microscopy, we generated mice with a germline deletion of layilin and crossed them to Foxp3-GFP reporter mice (61). Layilin-deficient mice (Layn$^{-/-}$) were created using CRISPR-Cas9 gene editing of C57BL/6 embryos (25). The single guide RNAs were designed against exon 1 and 4 and gene deletion in murine founder lines (backcrossed >2 generations to wildtype C57BL/6 mice) confirmed by layilin-specific PCR (Supplementary Figure S4A–B). Layn$^{-/-}$ mice had normal-sized litters with no gross abnormalities in growth or development (Supplementary Figure S4C). There were no obvious signs of spontaneous autoimmune disease and skin morphology appeared similar to WT mice (Supplementary Figure S4D). The percentage and absolute numbers of total CD45^{+} leukocytes as well as Tregs in skin and secondary lymphoid organs of Layn$^{-/-}$ mice revealed no abnormalities when compared to gender- and age-matched wildtype control animals (Supplementary Figure S4E–F). Additionally, there were no significant differences in expression of Treg activation markers, including CD25, ICOS, and CTLA-4, between Layn$^{-/-}$ and WT mice skin (Supplementary Figure S4G). Similar results were observed in LN and spleen (data not shown).

To test whether layilin expression influences the dynamic motility of Tregs in skin, we performed intravital 2-photon microscopy on Layn$^{-/-}$Foxp3^{GFP} mice. We utilized a unique vacuum suction approach for imaging intact dorsal skin, a method recently established by our laboratory (6). Mice were imaged at 8–10 weeks of age, a time point when there are maximum number of Tregs in skin of adult animals (6). When compared to control WT Foxp3^{GFP} mice, Tregs in dorsal skin of Layn$^{-/-}$ mice travelled longer distances at increased speeds, as measured by track displacement length and track speed mean (Figure 6A–C). Reduced sphericity is a marker of increased cell motility (62). Layn$^{-/-}$ Tregs exhibited a more amoeboid-like morphology with increased protrusive activity (Supplementary Videos 1 and 2). These differences in cell shape were quantified using Imaris software by rendering 3D surfaces on Tregs and applying a measure of relative sphericity (39). Layn$^{-/-}$ Tregs had significantly reduced sphericity as compared to WT Tregs at all the time points measured with a proportionate reduction in mean sphericity (Figure 6D–E). Taken together, these results indicate that Tregs in Layn$^{-/-}$ mice are less adherent and have increased motility in skin.

Because the experiments described above were performed in germline layn$^{-/-}$ mice, it is possible that layilin deficiency on a cell subset other than Tregs resulted in the observed differences in Treg motility. To determine if layilin expression on Tregs influences the motility of these cells in a cell-intrinsic fashion, we performed adoptive transfer experiments with Layn$^{-/-}$ Tregs. Immunodeficient RAG2$^{-/-}$ mice were adoptively transferred with Tregs from either Layn$^{-/-}$Foxp3^{GFP} mice or WT Foxp3^{GFP} controls, along with WT CD4^{+} Teff cells as a source of IL-2 needed for Treg survival in this model (63) (Figure 6F). Four to six weeks later, the skin of recipient mice was imaged using the intravital 2-photon approach described above (Supplementary Videos 3 and 4). Consistent with experiments performed in Layn$^{-/-}$/Foxp3^{GFP} mice, we observed that Layn$^{-/-}$ Tregs had significantly increased track displacement length and track speed mean as compared to WT Tregs (Figure 6G–I). These results validate experiments performed in Layn$^{-/-}$ mice and suggest that layilin expression on Tregs promotes their anchoring and adhesion in skin.

Discussion

Herein we show that the C-type lectin-like cell surface receptor, layilin, is expressed on a highly activated subset of Tregs in human skin. Layilin functions to anchor these cells, and in doing so, attenuates their suppressive capacity, without directly influencing their activation status. It seems somewhat paradoxical that the most activated tissue Tregs express a cell surface molecule that functions to attenuate their ability to regulate inflammation. However, this phenomenon is well established in other T cell subsets, as the most activated CD8^{+} T cells express the highest levels of the inhibitory receptors CTLA-4 and PD-1 (64, 65). This precedence has also been established for Tregs, as highly activated tissue Tregs have increased expression of LAG3 and PD-1, which may act to limit their suppressive potential (66–68). Thus, it is becoming increasingly appreciated that both the stimulatory and regulatory arms of the adaptive immune system utilize molecular pathways that act to limit their pro-inflammatory and anti-inflammatory functions, respectively, in an attempt to maintain immune homeostasis. These pathways may be most active in peripheral tissues,

where heightened immune reactivity or augmented immune suppression could have a major impact on organ function.

Receptors involved in cell-to-cell adhesion and/or adhesion of cells to the extracellular matrix have been shown to mediate inhibitory signals that limit cell function (15, 19, 20). The molecular mechanisms by which layilin attenuates Treg-mediated immune regulation are currently unknown. Our data suggest that the anchoring effect mediated by layilin limits the ability of Tregs to transverse through the skin. Consequently, these cells would likely have fewer interactions with other cells, resulting in an overall reduction in suppression, as many of the mechanisms Tregs utilize require close cell contact (69). This may explain why the effects of layilin expression on Tregs was more pronounced *in vivo* (Figure 2) than *in vitro* (Figure 3). This may also explain why we did not observe an effect of lack of layilin on Treg accumulation and suppression in steady state conditions (Figure S2 and data not shown), as it is only when the tissue becomes infiltrated by multiple immune cells that increased Treg mobility is required to achieve adequate suppression. We speculate that during inflammation, removing the anchoring effect of layilin on Tregs functions to create a more suppressive tissue microenvironment secondary to engagement of these cells with a greater number of inflammatory cells.

To the best of our knowledge, there is currently one published report examining the function of layilin on Tregs (70). These investigators transcriptionally profiled human Tregs expanded from peripheral blood and observed that *LAYN* was differentially expressed in these cells when compared to conventional $CD4^+$ T cells. Using an siRNA knockdown approach, they showed that Tregs treated with layilin siRNA were slightly more suppressive than control Tregs (treated with scrambled siRNA) in an *in vitro* Treg suppression assay. However, consistent with our findings, these results were quite modest with layilin having a minimal effect in these *in vitro* systems.

Functional manipulation of Tregs in tissues is emerging as an exciting area of translational biology. The role of layilin in influencing the accumulation and suppressive function of Tregs in non-lymphoid organs, and especially in our study in skin, make it a potentially attractive therapeutic target for autoimmunity or cancer. Our results provide the foundation for future studies focused on further understanding the molecular mechanisms underlying how layilin influences Treg biology as well as pharmacologic approaches aimed at either agonizing or antagonizing this pathway in pre-clinical animal models.

Supplementary Material

Refer to Web version on PubMed Central for supplementary material.

Acknowledgements

We thank the Biological Imaging Development Center for discussion and technical assistance with 2-photon imaging. We thank the UCSF Parnassus Flow Cytometry Core for help with generation of Flow Cytometry and Mass Cytometry data.

Declaration of Interests

M.D.R. is a co-founder and consultant for TRex Bio. which partially funded this research. He also is a cofounder of Sitryx Bio. W.L. and A.D. are co-founders of TRex Bio. P. Mankoo is employed by TRex Bio.

Flow Cytometry data was generated in the UCSF Parnassus Flow Cytometry Core that is supported by the Diabetes Research Center (DRC) grant NIH P30 DK063720. Mass cytometry data were generated in the UCSF Parnassus Flow Cytometry Core with support from NIH S10 1S10OD018040-01. This work was primarily funded by M.D.R's R21AR72195, Burroughs Wellcome Fund CAMS-1010934, NIH DP2-AR068130, Dermatology Foundation's Stiefel Scholar Award in Autoimmune & Connective Tissue Diseases grants, a research support grant sponsored by TRex Bio, and P.M.'s Dermatology Foundation Research Grant.

Abbreviations

CRISPR	Clustered Regularly Interspaced Short Palindromic Repeats
DT	Diptheria toxin
DTR	Diptheria toxin receptor
RAG-2	Recombination activating gene 2
sdLN	Skin draining lymph node
Teff	Effector T cells
Tregs	Regulatory T cells
DC	Dendritic Cells
KC	Keratinocytes

References

1. Panduro M, Benoist C, and Mathis D. 2016. Tissue Tregs. Annu.Rev.Immunol34: 609–633. [PubMed: 27168246]
2. Cipolletta D, Feuerer M, Li A, Kamei N, Lee J, Shoelson SE, Benoist C, and Mathis D. 2012. PPAR-gamma is a major driver of the accumulation and phenotype of adipose tissue Treg cells. Nature486: 549–553. [PubMed: 22722857]
3. Arpaia N, Green JA, Moltedo B, Arvey A, Hemmers S, Yuan S, Treuting PM, and Rudensky AY. 2015. A Distinct Function of Regulatory T Cells in Tissue Protection. Cell162: 1078–1089. [PubMed: 26317471]
4. Burzyn D, Kuswanto W, Kolodin D, Shadrach JL, Cerletti M, Jang Y, Sefik E, Tan TG, Wagers AJ, Benoist C, and Mathis D. 2013. A special population of regulatory T cells potentiates muscle repair. Cell155: 1282–1295. [PubMed: 24315098]
5. Villalta SA, Rosenthal W, Martinez L, Kaur A, Sparwasser T, Tidball JG, Margeta M, Spencer MJ, and Bluestone JA. 2014. Regulatory T cells suppress muscle inflammation and injury in muscular dystrophy. Sci.Transl.Med6: 258ra142.
6. Ali N, Zirak B, Rodriguez RS, Pauli ML, Truong HA, Lai K, Ahn R, Corbin K, Lowe MM, Scharschmidt TC, Taravati K, Tan MR, Ricardo-Gonzalez RR, Nosbaum A, Bertolini M, Liao W, Nestle FO, Paus R, Cotsarelis G, Abbas AK, and Rosenblum MD. 2017. Regulatory T Cells in Skin Facilitate Epithelial Stem Cell Differentiation. Cell169: 1119–1129. [PubMed: 28552347]
7. Mathur AN, Zirak B, Boothby IC, Tan M, Cohen JN, Mauro TM, Mehta P, Lowe MM, Abbas AK, Ali N, and Rosenblum MD. 2019. Treg-Cell Control of a CXCL5-IL-17 Inflammatory Axis Promotes Hair-Follicle-Stem-Cell Differentiation During Skin-Barrier Repair. Immunity50: 655–667.e4. [PubMed: 30893588]

8. Kalekar LA, Cohen JN, Prevel N, Sandoval PM, Mathur AN, Moreau JM, Lowe MM, Nosbaum A, Wolters PJ, Haemel A, Boin F, and Rosenblum MD. 2019. Regulatory T cells in skin are uniquely poised to suppress profibrotic immune responses. Sci. Immunol4.

9. Chow Z, Mueller SN, Deane JA, and Hickey MJ. 2013. Dermal regulatory T cells display distinct migratory behavior that is modulated during adaptive and innate inflammation. J. Immunol. Baltim. Md 1950191: 3049–3056.

10. Gratz IK, Truong HA, Yang SH, Maurano MM, Lee K, Abbas AK, and Rosenblum MD. 2013. Cutting Edge: memory regulatory t cells require IL-7 and not IL-2 for their maintenance in peripheral tissues. J.Immunol190: 4483–4487. [PubMed: 23543753]

11. Sanchez RR, Pauli ML, Neuhaus IM, Yu SS, Arron ST, Harris HW, Yang SH, Anthony BA, Sverdrup FM, Krow-Lucal E, MacKenzie TC, Johnson DS, Meyer EH, Lohr A, Hsu A, Koo J, Liao W, Gupta R, Debbaneh MG, Butler D, Huynh M, Levin EC, Leon A, Hoffman WY, McGrath MH, Alvarado MD, Ludwig CH, Truong HA, Maurano MM, Gratz IK, Abbas AK, and Rosenblum MD. 2014. Memory regulatory T cells reside in human skin. J.Clin.Invest124: 1027–1036. [PubMed: 24509084]

12. Maynard CL, Harrington LE, Janowski KM, Oliver JR, Zindl CL, Rudensky AY, and Weaver CT. 2007. Regulatory T cells expressing interleukin 10 develop from Foxp3+ and Foxp3- precursor cells in the absence of interleukin 10. Nat. Immunol8: 931–941. [PubMed: 17694059]

13. Smigiel KS, Richards E, Srivastava S, Thomas KR, Dudda JC, Klonowski KD, and Campbell DJ. 2014. CCR7 provides localized access to IL-2 and defines homeostatically distinct regulatory T cell subsets. J. Exp. Med211: 121–136. [PubMed: 24378538]

14. Jankowska KI, Williamson EK, Roy NH, Blumenthal D, Chandra V, Baumgart T, and Burkhardt JK. 2018. Integrins Modulate T Cell Receptor Signaling by Constraining Actin Flow at the Immunological Synapse. Front. Immunol9: 25. [PubMed: 29403502]

15. Schittenhelm L, Hilkens CM, and Morrison VL. 2017. β2 Integrins As Regulators of Dendritic Cell, Monocyte, and Macrophage Function. Front. Immunol8: 1866. [PubMed: 29326724]

16. Han C, Jin J, Xu S, Liu H, Li N, and Cao X. 2010. Integrin CD11b negatively regulates TLR-triggered inflammatory responses by activating Syk and promoting degradation of MyD88 and TRIF via Cbl-b. Nat. Immunol11: 734–742. [PubMed: 20639876]

17. Morrison VL, James MJ, Grzes K, Cook P, Glass DG, Savinko T, Lek HS, Gawden-Bone C, Watts C, Millington OR, MacDonald AS, and Fagerholm SC. 2014. Loss of beta2-integrin-mediated cytoskeletal linkage reprogrammes dendritic cells to a mature migratory phenotype. Nat. Commun5: 5359. [PubMed: 25348463]

18. Yee NK, and Hamerman JA. 2013. β(2) integrins inhibit TLR responses by regulating NF-κB pathway and p38 MAPK activation. Eur. J. Immunol43: 779–792. [PubMed: 23310953]

19. Dai B, Wu P, Xue F, Yang R, Yu Z, Dai K, Ruan C, Liu G, Newman PJ, and Gao C. 2016. Integrin-αIIbβ3-mediated outside-in signalling activates a negative feedback pathway to suppress platelet activation. Thromb. Haemost116: 918–930. [PubMed: 27465472]

20. Redelinghuys P, and Brown GD. 2011. Inhibitory C-type lectin receptors in myeloid cells. Immunol. Lett136: 1–12. [PubMed: 20934454]

21. Bono P, Cordero E, Johnson K, Borowsky M, Ramesh V, Jacks T, and Hynes RO. 2005. Layilin, a cell surface hyaluronan receptor, interacts with merlin and radixin. ExpCell Res308: 177–187.

22. Borowsky ML, and Hynes RO. 1998. Layilin, a novel talin-binding transmembrane protein homologous with C-type lectins, is localized in membrane ruffles. JCell Biol143: 429–442. [PubMed: 9786953]

23. Chen Z, Zhuo W, Wang Y, Ao X, and An J. 2008. Down-regulation of layilin, a novel hyaluronan receptor, via RNA interference, inhibits invasion and lymphatic metastasis of human lung A549 cells. Biotechnol.Appl.Biochem50: 89–96. [PubMed: 17822380]

24. Mahuron KM, Moreau JM, Glasgow JE, Boda DP, Pauli ML, Gouirand V, Panjabi L, Grewal R, Luber JM, Mathur AN, Feldman RM, Shifrut E, Mehta P, Lowe MM, Alvarado MD, Marson A, Singer M, Wells J, Jupp R, Daud AI, and Rosenblum MD. 2020. Layilin augments integrin activation to promote antitumor immunity. J. Exp. Med217.

25. Cong L, Ran FA, Cox D, Lin S, Barretto R, Habib N, Hsu PD, Wu X, Jiang W, Marraffini LA, and Zhang F. 2013. Multiplex genome engineering using CRISPR/Cas systems. Science339: 819–823. [PubMed: 23287718]
26. Trapnell C, Pachter L, and Salzberg SL. 2009. TopHat: discovering splice junctions with RNA-Seq. Bioinformatics. 25: 1105–1111. [PubMed: 19289445]
27. Li H, Handsaker B, Wysoker A, Fennell T, Ruan J, Homer N, Marth G, Abecasis G, and Durbin R. 2009. The Sequence Alignment/Map format and SAMtools. Bioinformatics. 25: 2078–2079. [PubMed: 19505943]
28. Love MI, Huber W, and Anders S. 2014. Moderated estimation of fold change and dispersion for RNA-seq data with DESeq2. Genome Biol15: 550. [PubMed: 25516281]
29. Ahn RS, Taravati K, Lai K, Lee KM, Nititham J, Gupta R, Chang DS, Arron ST, Rosenblum M, and Liao W. 2017. Transcriptional landscape of epithelial and immune cell populations revealed through FACS-seq of healthy human skin. Sci.Rep7: 1343. [PubMed: 28465541]
30. Tang Q, Henriksen KJ, Bi M, Finger EB, Szot G, Ye J, Masteller EL, McDevitt H, Bonyhadi M, and Bluestone JA. 2004. In Vitro–expanded Antigen-specific Regulatory T Cells Suppress Autoimmune Diabetes. J. Exp. Med199: 1455–1465. [PubMed: 15184499]
31. Spitzer MH, Gherardini PF, Fragiadakis GK, Bhattacharya N, Yuan RT, Hotson AN, Finck R, Carmi Y, Zunder ER, Fantl WJ, Bendall SC, Engleman EG, and Nolan GP. 2015. IMMUNOLOGY. An interactive reference framework for modeling a dynamic immune system. Science349: 1259425. [PubMed: 26160952]
32. Finck R, Simonds EF, Jager A, Krishnaswamy S, Sachs K, Fantl W, Pe'er D, Nolan GP, and Bendall SC. 2013. Normalization of mass cytometry data with bead standards. Cytom. Part J. Int. Soc. Anal. Cytol83: 483–494.
33. Nowicka M, Krieg C, Crowell HL, Weber LM, Hartmann FJ, Guglietta S, Becher B, Levesque MP, and Robinson MD. 2017. CyTOF workflow: differential discovery in high-throughput high-dimensional cytometry datasets. F1000Research6: 748. [PubMed: 28663787]
34. Collison LW, Chaturvedi V, Henderson AL, Giacomin PR, Guy C, Bankoti J, Finkelstein D, Forbes K, Workman CJ, Brown SA, Rehg JE, Jones ML, Ni H-T, Artis D, Turk MJ, and Vignali DAA. 2010. IL-35-mediated induction of a potent regulatory T cell population. Nat. Immunol11: 1093–1101. [PubMed: 20953201]
35. Faustino-Rocha A, Oliveira PA, Pinho-Oliveira J, Teixeira-Guedes C, Soares-Maia R, da Costa RG, Colaço B, Pires MJ, Colaço J, Ferreira R, and Ginja M. 2013. Estimation of rat mammary tumor volume using caliper and ultrasonography measurements. Lab Anim. 42: 217–224.
36. Scharschmidt TC, Vasquez KS, Truong HA, Gearty SV, Pauli ML, Nosbaum A, Gratz IK, Otto M, Moon JJ, Liese J, Abbas AK, Fischbach MA, and Rosenblum MD. 2015. A Wave of Regulatory T Cells into Neonatal Skin Mediates Tolerance to Commensal Microbes. Immunity. 43: 1011–1021. [PubMed: 26588783]
37. Collison LW, and Vignali DAA. 2011. In vitro Treg suppression assays. Methods Mol. Biol. Clifton NJ707: 21–37.
38. Bullen A, Friedman RS, and Krummel MF. 2009. Two-photon imaging of the immune system: a custom technology platform for high-speed, multicolor tissue imaging of immune responses. Curr.Top.Microbiol.Immunol334: 1–29. [PubMed: 19521679]
39. Thornton EE, Looney MR, Bose O, Sen D, Sheppard D, Locksley R, Huang X, and Krummel MF. 2012. Spatiotemporally separated antigen uptake by alveolar dendritic cells and airway presentation to T cells in the lung. J.Exp.Med209: 1183–1199. [PubMed: 22585735]
40. Pinkard H, Stuurman N, Corbin K, Vale R, and Krummel MF. 2016. Micro-Magellan: open-source, sample-adaptive, acquisition software for optical microscopy. Nat.Methods13: 807–809. [PubMed: 27684577]
41. Hori S, Nomura T, and Sakaguchi S. 2003. Control of regulatory T cell development by the transcription factor Foxp3. Science299: 1057–1061. [PubMed: 12522256]
42. Hill JA, Feuerer M, Tash K, Haxhinasto S, Perez J, Melamed R, Mathis D, and Benoist C. 2007. Foxp3 transcription-factor-dependent and -independent regulation of the regulatory T cell transcriptional signature. Immunity. 27: 786–800. [PubMed: 18024188]

43. Jabri B, and Abadie V. 2015. IL-15 functions as a danger signal to regulate tissue-resident T cells and tissue destruction. Nat. Rev. Immunol15: 771–783. [PubMed: 26567920]
44. Liu Y, Ma C, and Zhang N. 2018. Tissue-Specific Control of Tissue-Resident Memory T Cells. Crit. Rev. Immunol38: 79–103. [PubMed: 29953389]
45. Travis MA, and Sheppard D. 2014. TGF-β activation and function in immunity. Annu. Rev. Immunol32: 51–82. [PubMed: 24313777]
46. Cong L, Ran FA, Cox D, Lin S, Barretto R, Habib N, Hsu PD, Wu X, Jiang W, Marraffini LA, and Zhang F. 2013. Multiplex Genome Engineering Using CRISPR/Cas Systems. Science339: 819–823. [PubMed: 23287718]
47. Borowsky ML, and Hynes RO. 1998. Layilin, a novel talin-binding transmembrane protein homologous with C- type lectins, is localized in membrane ruffles. J. Cell Biol143: 429–442. [PubMed: 9786953]
48. Rubtsov YP, Rasmussen JP, Chi EY, Fontenot J, Castelli L, Ye X, Treuting P, Siewe L, Roers A, Henderson WR, Muller W, and Rudensky AY. 2008. Regulatory T cell-derived interleukin-10 limits inflammation at environmental interfaces. Immunity28: 546–558. [PubMed: 18387831]
49. Rubtsov YP, Niec RE, Josefowicz S, Li L, Darce J, Mathis D, Benoist C, and Rudensky AY. 2010. Stability of the regulatory T cell lineage in vivo. Science329: 1667–1671. [PubMed: 20929851]
50. De SM, Arrigoni A, Rossetti G, Gruarin P, Ranzani V, Politano C, Bonnal RJ, Provasi E, Sarnicola ML, Panzeri I, Moro M, Crosti M, Mazzara S, Vaira V, Bosari S, Palleschi A, Santambrogio L, Bovo G, Zucchini N, Totis M, Gianotti L, Cesana G, Perego RA, Maroni N, Pisani CA, Opocher E, De FR, Geginat J, Stunnenberg HG, Abrignani S, and Pagani M. 2016. Transcriptional Landscape of Human Tissue Lymphocytes Unveils Uniqueness of Tumor-Infiltrating T Regulatory Cells. Immunity. 45: 1135–1147. [PubMed: 27851914]
51. Guo X, Zhang Y, Zheng L, Zheng C, Song J, Zhang Q, Kang B, Liu Z, Jin L, Xing R, Gao R, Zhang L, Dong M, Hu X, Ren X, Kirchhoff D, Roider HG, Yan T, and Zhang Z. 2018. Global characterization of T cells in non-small-cell lung cancer by single-cell sequencing. Nat. Med24: 978–985. [PubMed: 29942094]
52. Zheng C, Zheng L, Yoo JK, Guo H, Zhang Y, Guo X, Kang B, Hu R, Huang JY, Zhang Q, Liu Z, Dong M, Hu X, Ouyang W, Peng J, and Zhang Z. 2017. Landscape of Infiltrating T Cells in Liver Cancer Revealed by Single-Cell Sequencing. Cell169: 1342–1356. [PubMed: 28622514]
53. Delgoffe GM, Woo S-R, Turnis ME, Gravano DM, Guy C, Overacre AE, Bettini ML, Vogel P, Finkelstein D, Bonnevier J, Workman CJ, and Vignali DAA. 2013. Stability and function of regulatory T cells is maintained by a neuropilin-1–semaphorin-4a axis. Nature501: 252–256. [PubMed: 23913274]
54. Nishikawa H, and Sakaguchi S. 2010. Regulatory T cells in tumor immunity. Int. J. Cancer127: 759–767. [PubMed: 20518016]
55. Bono P, Rubin K, Higgins JM, and Hynes RO. 2001. Layilin, a novel integral membrane protein, is a hyaluronan receptor. Mol.Biol.Cell12: 891–900. [PubMed: 11294894]
56. Nosbaum A, Prevel N, Truong H-A, Mehta P, Ettinger M, Scharschmidt TC, et al.Cutting Edge: Regulatory T Cells Facilitate Cutaneous Wound Healing. J. ImmunolThe American Association of Immunologists; 2016;196(5):2010–4 [PubMed: 26826250]
57. Delacher M, Imbusch CD, Hotz-Wagenblatt A, Mallm J-P, Bauer K, Simon M, Riegel D, Rendeiro AF, Bittner S, Sanderink L, Pant A, Schmidleithner L, Braband KL, Echtenachter B, Fischer A, Giunchiglia V, Hoffmann P, Edinger M, Bock C, Rehli M, Brors B, Schmidl C, and Feuerer M. 2020. Precursors for Nonlymphoid-Tissue Treg Cells Reside in Secondary Lymphoid Organs and Are Programmed by the Transcription Factor BATF. Immunity.
58. van, der V, Gonzalez AJ, Cho H, Arvey A, Hemmers S, Leslie CS, and Rudensky AY. 2016. Memory of Inflammation in Regulatory T Cells. Cell166: 977–990. [PubMed: 27499023]
59. Wyss L, Stadinski BD, King CG, Schallenberg S, McCarthy NI, Lee JY, Kretschmer K, Terracciano LM, Anderson G, Surh CD, Huseby ES, and Palmer E. 2016. Affinity for self antigen selects Treg cells with distinct functional properties. Nat.Immunol17: 1093–1101. [PubMed: 27478940]
60. Kim JM, Rasmussen JP, and Rudensky AY. 2007. Regulatory T cells prevent catastrophic autoimmunity throughout the lifespan of mice. Nat.Immunol8: 191–197. [PubMed: 17136045]

61. Lin W, Haribhai D, Relland LM, Truong N, Carlson MR, Williams CB, and Chatila TA. 2007. Regulatory T cell development in the absence of functional Foxp3. Nat.Immunol8: 359–368. [PubMed: 17273171]

62. Lecuit T, and Lenne PF. 2007. Cell surface mechanics and the control of cell shape, tissue patterns and morphogenesis. NatRevMolCell Biol8: 633–644.

63. Duarte JH, Zelenay S, Bergman ML, Martins AC, and Demengeot J. 2009. Natural Treg cells spontaneously differentiate into pathogenic helper cells in lymphopenic conditions. Eur.J.Immunol39: 948–955. [PubMed: 19291701]

64. Barber DL, Wherry EJ, Masopust D, Zhu B, Allison JP, Sharpe AH, Freeman GJ, and Ahmed R. 2006. Restoring function in exhausted CD8 T cells during chronic viral infection. Nature439: 682–687. [PubMed: 16382236]

65. Wherry EJ, Ha S-J, Kaech SM, Haining WN, Sarkar S, Kalia V, Subramaniam S, Blattman JN, Barber DL, and Ahmed R. 2007. Molecular signature of CD8+ T cell exhaustion during chronic viral infection. Immunity27: 670–684. [PubMed: 17950003]

66. Kamada T, Togashi Y, Tay C, Ha D, Sasaki A, Nakamura Y, Sato E, Fukuoka S, Tada Y, Tanaka A, Morikawa H, Kawazoe A, Kinoshita T, Shitara K, Sakaguchi S, and Nishikawa H. 2019. PD-1+ regulatory T cells amplified by PD-1 blockade promote hyperprogression of cancer. Proc. Natl. Acad. Sci. U. S. A116: 9999–10008. [PubMed: 31028147]

67. Zhang B, Chikuma S, Hori S, Fagarasan S, and Honjo T. 2016. Nonoverlapping roles of PD-1 and FoxP3 in maintaining immune tolerance in a novel autoimmune pancreatitis mouse model. Proc. Natl. Acad. Sci. U. S. A113: 8490–8495. [PubMed: 27410049]

68. Zhang Q, Chikina M, Szymczak-Workman AL, Horne W, Kolls JK, Vignali KM, Normolle D, Bettini M, Workman CJ, and Vignali DAA. 2017. LAG3 limits regulatory T cell proliferation and function in autoimmune diabetes. Sci. Immunol2.

69. Yamaguchi T, Wing JB, and Sakaguchi S. 2011. Two modes of immune suppression by Foxp3(+) regulatory T cells under inflammatory or non-inflammatory conditions. Semin. Immunol23: 424–430. [PubMed: 22055883]

70. Bhairavabhotla R, Kim YC, Glass DD, Escobar TM, Patel MC, Zahr R, Nguyen CK, Kilaru GK, Muljo SA, and Shevach EM. 2016. Transcriptome profiling of human FoxP3+ regulatory T cells. Hum. Immunol77: 201–213. [PubMed: 26686412]

Key findings:

- Layilin is expressed by highly activated Tregs in healthy and diseased human skin
- *In vivo*, layilin attenuates Treg suppressive capacity
- Layilin contributes to ‘Anchor’ Tregs in skin and enhances their accumulation

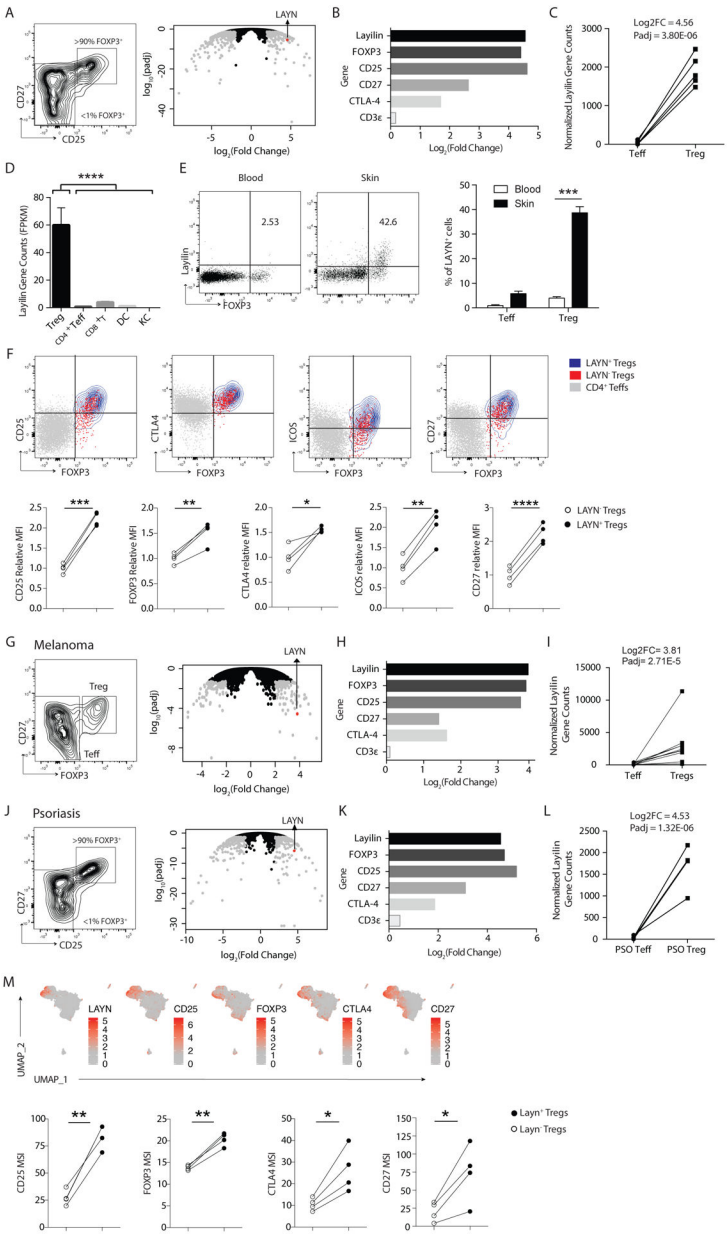

Figure 1. Layilin is preferentially and highly expressed on a subset of activated Tregs in healthy and diseased human skin.

(a-c) RNA-Seq of Tregs and Teff cells FACS-purified from normal human skin. **(a)** Tregs and Teffs were sorted purifed based on CD25 and CD27 expression. A representative flow plot is shown. Cells were pre-gated on live $CD45^{+}CD3^{+}CD4^{+}CD8^{-}$ cells. Volcano plot comparing expression profile of Tregs versus Teffs is shown. **(b)** Expression of specific genes identified by RNA-Seq, including layilin, Foxp3, CD27, CTLA-4, CD25 and CD3ε, by skin Tregs relative to skin Teffs. **(c)** Gene counts of layilin transcipts on Teff and Tregs. n = 5 healthy donors. **(d)** Layilin expression on Tregs, $CD4^{+}$ Teffs, $CD8^{+}$ T cells, dendritic cells (DC) and keratinocytes (KC), sort-purified from normal human skin, as determined by RNA-Seq. n = 7 normal healthy donors. ANOVA used for analysis. **(e)** Flow cytometric analysis of percentage of $layilin^{+}$ cells within $CD4^{+}Foxp3^{+}$ Tregs and $CD4^{+}Foxp3^{-}$ Teff

populations in human skin versus peripheral blood. n = 5–12 healthy donors/group. **(f)** Flow cytometric analysis of median fluorescence intensity (MFI) of CD25, Foxp3, CTLA4, ICOS and CD27 expression on Layn^{high} Tregs, Layn^{low} Tregs, and CD4^{+} Teff in human skin. n = 4 healthy donors. Representative flow plots and their quantification for Tregs is shown. **(g-i)** RNA-Seq analysis of Tregs and Teffs FACS-purified from metastatic tumors of melanoma patients. n = 12 melanoma patients. **(j-l)** RNA-Seq analysis of Tregs and Teffs FACS-purified from lesional skin of psoriasis patients. n = 4–5 psoriasis patients. **(m)** Uniform Manifold Approximation and Projection (UMAP) embeddings of mass cytometric data with indicated scaled marker intensities. Gated CD4+ T cells (n = 11,465 cells) were proportionally sampled from 4 lesional psoriasis skin punch biopsies (top). Paired median signal intensities (MSI) of CD25, FOXP3, CTLA4, and CD27 on LAYN+ and LAYN- Tregs (bottom).

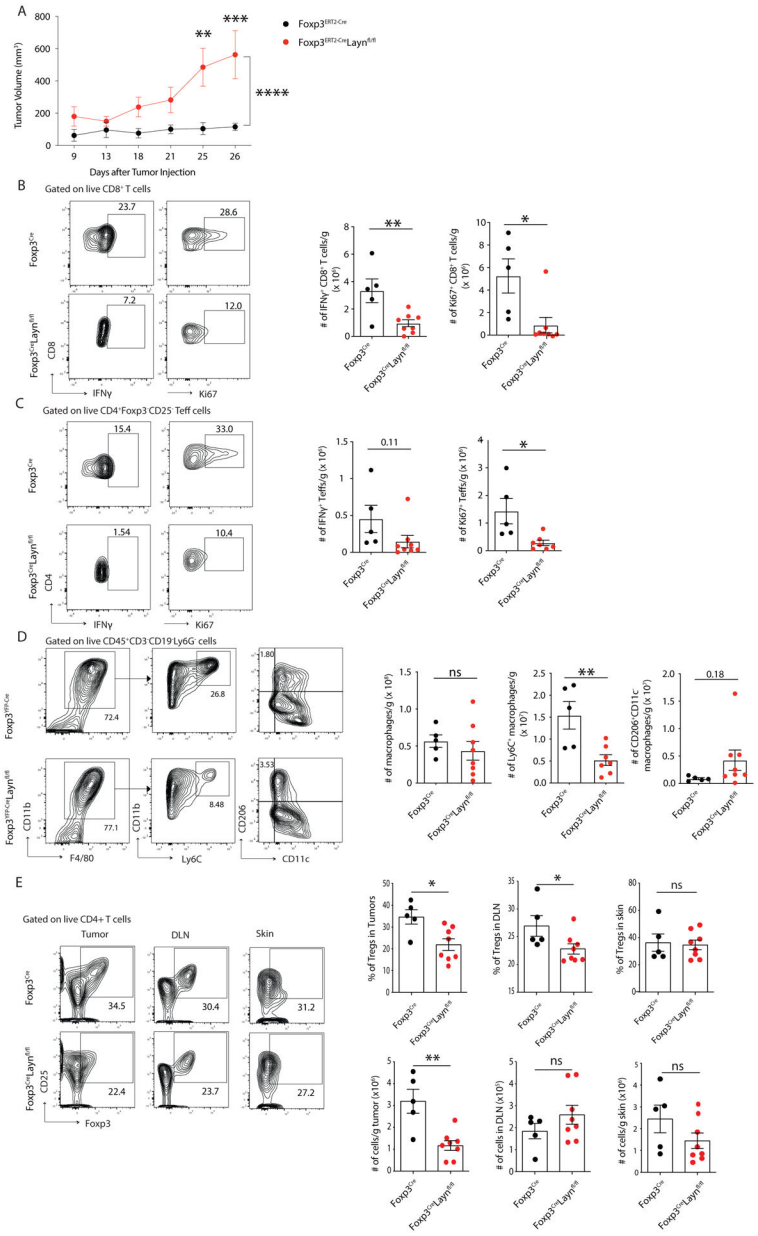

Figure 2. Layilin attenuates Treg suppressive capacity in vivo.

(a) Foxp3^{Cre}Layn$^{fl/fl}$ or control Foxp3^{Cre} mice both treated with tamoxifen were injected s.c. with the MC38 tumor cell line and tumor growth quantified by caliper measurements over time. n = 7–8 mice/group. Data representative of 2 independent experiments. Two-way ANOVA with Bonferroni's test for multiple comparisons. **(b-e)** Flow cytometric analysis of specific leukocyte populations in specified tissues of Foxp3^{Cre}Layn$^{fl/fl}$ or control Foxp3^{Cre} mice, 24 days after MC38 tumor engraftment. **(b)** IFNγ^+ and Ki67$^+$ CD8$^+$ T cells, **(c)** IFNγ^+ and Ki67$^+$ CD4$^+$ Teff cells, and **(d)** total, Ly6C$^+$, and CD206$^+$CD11c$^-$ macrophages, infiltrating tumors. **(e)** Live CD4$^+$CD25$^+$Foxp3$^+$ Tregs in tumor, tumor draining lymph nodes (DLN) and skin. Representative flow plots and their quantification is shown. Data representative of 3 independent experiments. n = 5–8 mice/group. Unpaired Student's t-test.

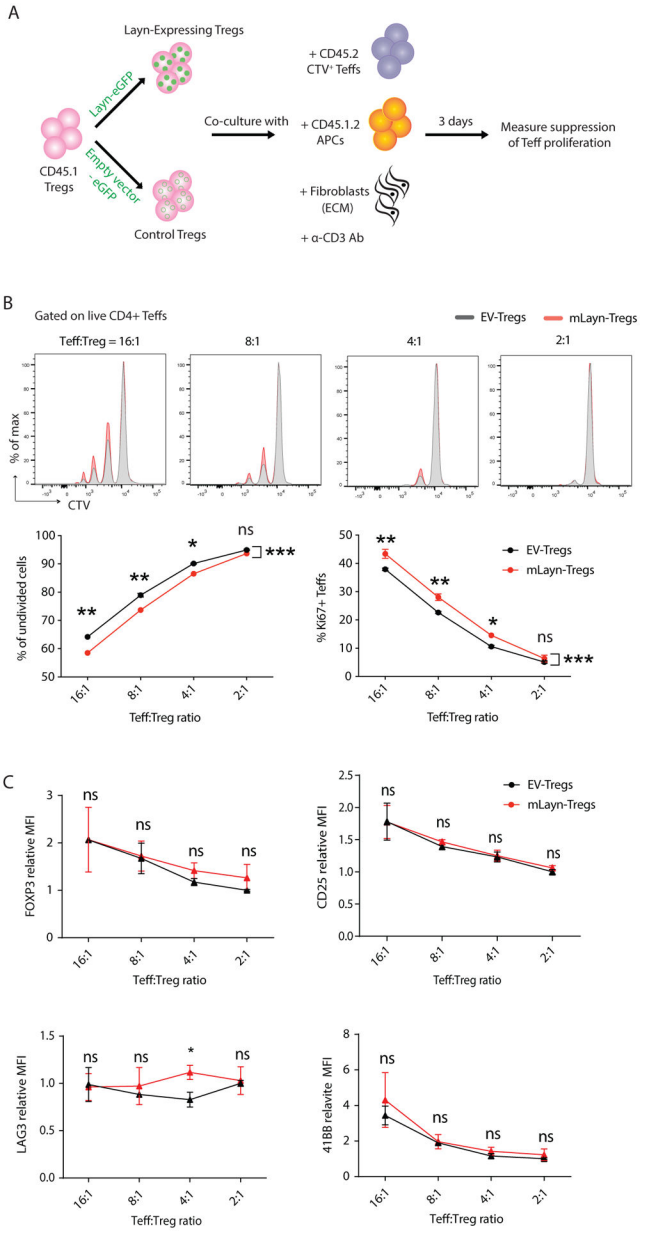

Figure 3. Layilin plays a minor role in Treg-mediated suppression *in vitro*.

(a) Experimental scheme. CTV-stained Teffs were cocultured with varying proportions of sorted Tregs retrovirally transduced with either Layn-eGFP-pMIG vector (mLayn-Treg) or empty pMIG vector (EV-Treg), in the presence of mitomycin C-treated APCs and 0.5ug/ml α-CD3 on a fibroblast-coated plate for 72 hours. **(b)** Representative histograms and quantification of Teff proliferation, as measured by percentage of undivided Teffs and proliferating Teffs (% of $Ki67^+$ Teffs). **(c)** Treg activation status. Flow cytometric analysis of MFI of FOXP3, CD25, 41BB and LAG3 expression on mLayn-Tregs compared to EV-Tregs, during suppression assay. n = 3 replicates/condition. Data representative of 4 independent experiments. Two-way ANOVA with Bonferroni's test for multiple comparisons.

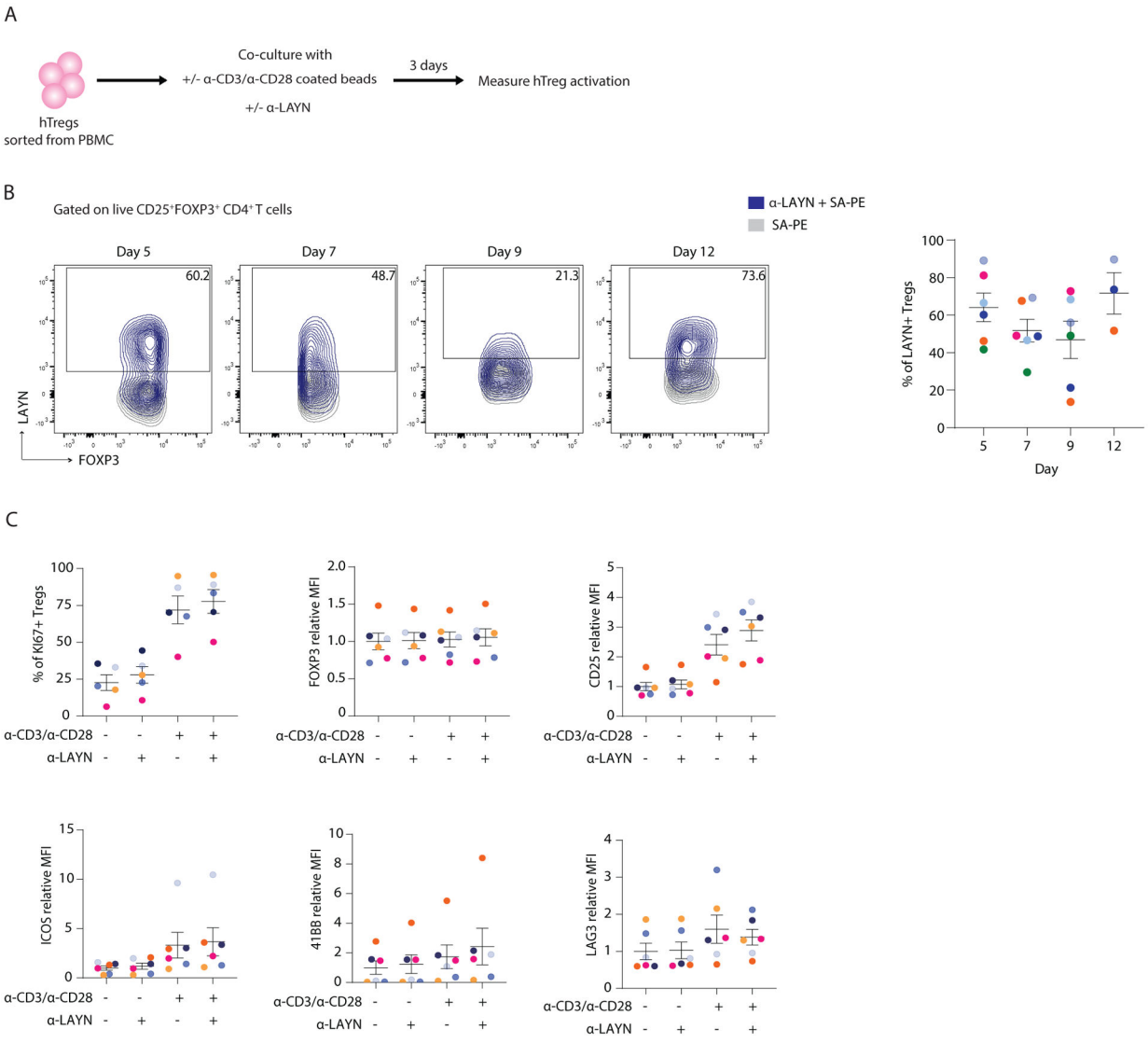

Figure 4. Layilin crosslinking on human Tregs has no significant impact on Treg activation *in vitro*.

(a) Experimental scheme for c. Tregs were sort purified from peripheral blood of healthy human donors and expanded for 9 or 14 days with α-CD3/CD28 beads and IL-2. Cells were then rested overnight and re-stimulated for 3 days with or without layilin cross-linking antibody, in the presence or absence of α-CD3/CD28 beads. **(b)** Flow cytometric quantification of expression of layilin over time on Tregs sort purified from peripheral blood and expanded *ex vivo* with α-CD3/CD28 coated beads and high dose IL-2. Data presented as % of $LAYN^+$ Tregs over time. **(c)** Flow cytometric quantification of % of $Ki67^+$ Tregs and MFI of FOXP3, CD25, ICOS, 4–1BB and LAG3 expression on *ex vivo* expanded Tregs after 3 days of coculture as outlined in a. Results are combined data from 4 donors for b and 3 donors for c with 1–2 donors repeated twice or thrice. Donors are color-coded. One-way ANOVA with Bonferroni's test for multiple comparisons.

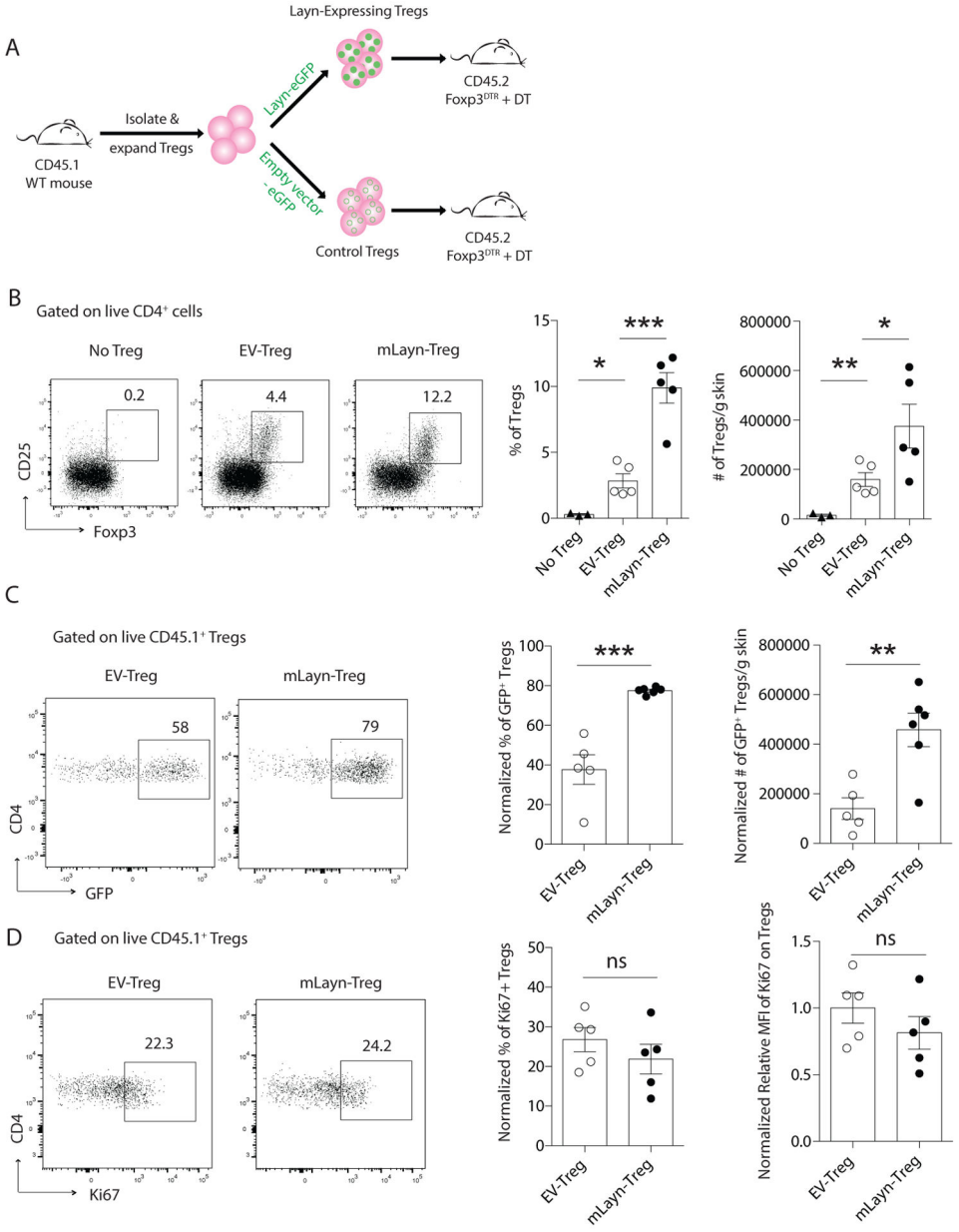

Figure 5. Layilin expression on Tregs promotes their accumulation in tissues.

(a-d) Adoptive transfer of Layn-overexpressing Tregs into Foxp3^{DTR} mice. **(a)** Experimental scheme. Tregs sorted from CD45.1 mice were expanded *ex vivo* and retrovirally transduced with either Layn-eGFP-pMIG vector or empty-eGFP pMIG vector. These cells were *i.v.* injected into 6–10 weeks old CD45.2 Foxp3^{DTR} mice and host Tregs depleted through administration of DT. **(b-d)** Flow cytometric quantification of total CD4^{+}CD25^{+}Foxp3^{+} Tregs in CD45.2 Foxp3^{DTR} mice and host Tregs depleted through administration of DT non-injected with Tregs or *i.v.* injected with mLayn- or EV-Tregs **(b),** and GFP^{+}CD45.1^{+} Tregs **(c)** in skin of CD45.2 Foxp3^{DTR} mice, represented as percentages and absolute number of cells, normalized to transfection efficiency. **(d)** Expression of Ki67 on CD45.1^{+}

Tregs in skin of CD45.2 Foxp3^{DTR} mice. Data representative of 3 independent experiments. n = 3–5 mice/group. Unpaired Student's t-test.

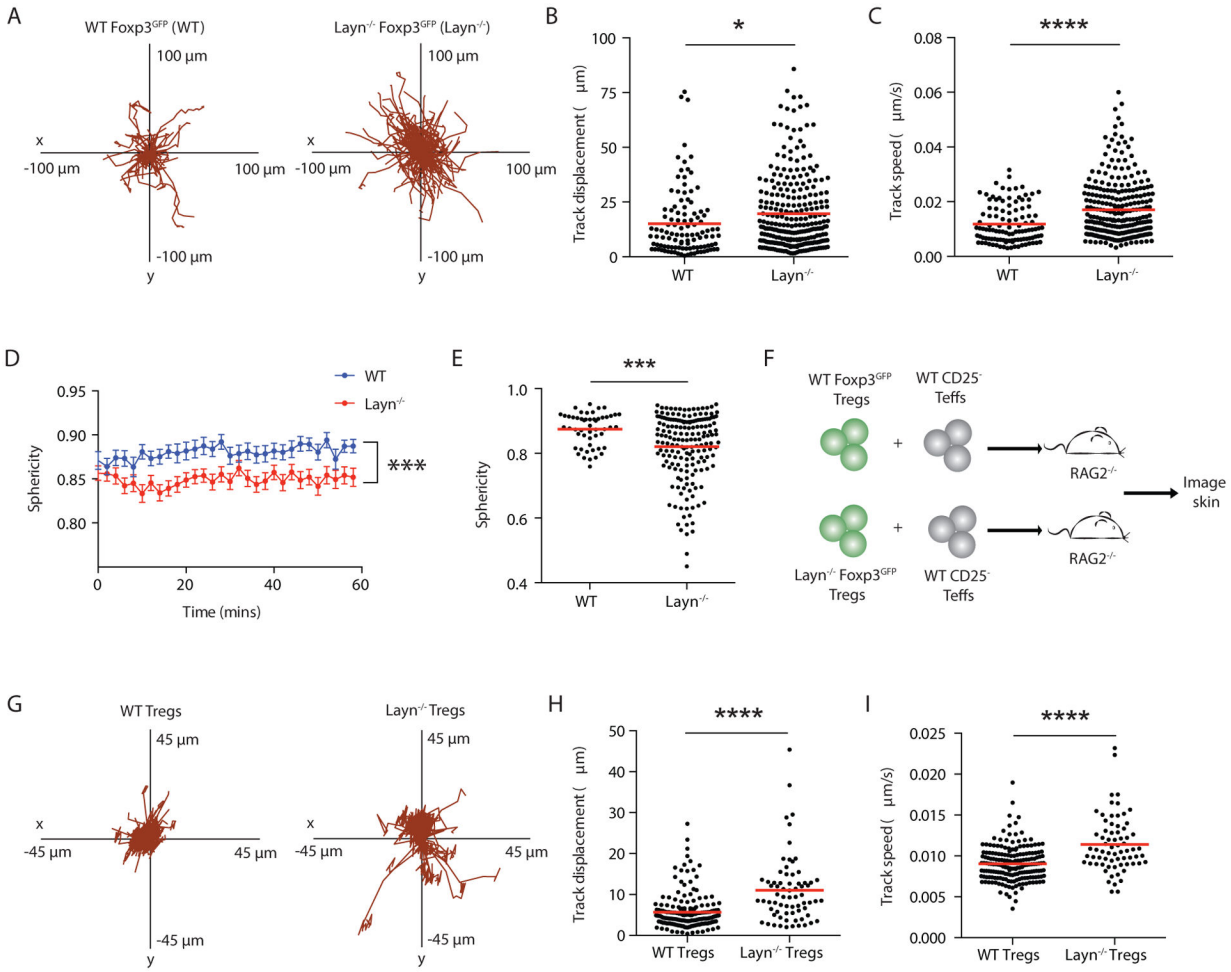

Figure 6. Layilin functions to 'anchor' Tregs in skin.

(a-d) Intravital two-photon imaging of Tregs in skin of Layn$^{-/-}$ Foxp3^{GFP} mice compared to WT Foxp3^{GFP} mice at steady state, over a period of 60 minutes. **(a)** xy plots of cell tracks, **(b)** track displacement length, **(c)** track speed means of the tracks, **(d)** sphericity of cells over time and **(e)** mean sphericity of each cell. **(f-i)** Intravital two-photon imaging of Tregs in skin of RAG2$^{-/-}$ mice 6 weeks after being adoptively transferred with Tregs from either Layn$^{-/-}$ Foxp3^{GFP} mice or WT Foxp3^{GFP} mice, over a period of 60 minutes. **(f)** Experimental scheme of adoptive transfer of cells. **(g)** xy plots of cell tracks, **(h)** track displacement length, and **(i)** track speed means of the tracks. n = at least 100 cells/group. Data representative of 2–3 independent experiments. Unpaired Student's t-test.